

Dramatic enhancement of structure-borne wave energy harvesting using an elliptical acoustic mirror

M. Carrara,¹ M. R. Cacan,² M. J. Leamy,² M. Ruzzene,^{1,2} and A. Erturk^{2,a)}

¹*D. Guggenheim School of Aerospace Engineering, Georgia Institute of Technology, Atlanta, Georgia 30332, USA*

²*G. W. Woodruff School of Mechanical Engineering, Georgia Institute of Technology, Atlanta, Georgia 30332, USA*

(Received 25 March 2012; accepted 30 April 2012; published online 18 May 2012)

Broadband structure-borne wave energy harvesting is reported by wave focusing using an elliptical acoustic mirror (EAM). The EAM is formed by an array of cylindrical stubs mounted along a semi-elliptical path on the surface of a plate. The array back-scatters incoming guided waves and focuses them at the focal location where a piezoelectric energy harvester is located. Multiple scattering simulations and experiments illustrate the broadband focusing characteristics of the EAM. More than an order of magnitude improvement in piezoelectric power generation is documented for an EAM-based energy harvester with respect to a free harvester over the 30–70 kHz frequency range. © 2012 American Institute of Physics. [<http://dx.doi.org/10.1063/1.4719098>]

The harvesting of waste mechanical energy for low-power electricity generation has been heavily researched over the past decade.^{1,2} The ultimate goal in energy harvesting research is to enable self-powered wireless electronic components, such as integrated sensor nodes used for structural health assessment, by eliminating the need for battery replacement and disposal. Although the harvesting of direct vibrational energy has been well studied through piezoelectric,^{3–6} electrostatic,^{7,8} electromagnetic,^{9,10} and magnetostrictive^{11,12} transduction mechanisms as well as by electroactive polymers,^{13,14} limited effort has been devoted to exploiting the energy of propagating waves in structures and fluids. Only a few research groups have addressed this area with the use of Helmholtz resonators,¹⁵ sonic crystals,¹⁶ and polarization-patterned piezoelectric solids¹⁷ for structure-borne or air-borne wave energy harvesting. Others have investigated aeroelastic and hydroelastic phenomena for flow energy harvesting.^{18–21}

Harvesting propagating waves in structures can be enhanced through arrays of acoustic scatterers designed to focus or properly localize the associated acoustic energy. Periodic layouts of scatterers often form the basis for the implementation of acoustic metamaterials,^{22,23} in addition to the achievement of unique wave propagation properties such as the presence of frequency bandgaps, response directionality or wave “beaming,” left-handedness, and negative acoustic refraction.^{24–27}

In this work, an array of acoustic scatterers laid out along an elliptical path is proposed as an effective way of focusing propagating waves. The scatterers consist of cylindrical stubs mounted on the surface of a plate, which supports the propagation of Lamb waves. The resulting elliptical acoustic mirror (EAM) is employed for performance enhancement in structure-borne wave energy harvesting. The goal is to implement a configuration that can capture and

focus the incoming wave energy at a specific point in space (precisely the focus of the ellipse) where the energy harvester is located to maximize the electrical power output. Periodically stubbed plates have been extensively investigated as examples of acoustic metamaterials featuring bandgaps generated through Bragg scattering,²³ or by the low-frequency resonance of soft stubs.²⁸ In the proposed EAM, the arrangement of the stubs is selected with the goal of achieving broadband focusing capabilities and enhanced energy harvesting performance. The elliptical arrangement of the stubs ensures focusing of waves emanating from a point source, while the spacing of the stubs along the ellipse is smaller or of the order of the wavelength of the considered Lamb wave mode in the frequency range of interest, so that the array behaves approximately as a perfect acoustic mirror. Therefore, the concept of EAM-based structure-borne wave energy harvesting presented herein employs the acoustic mirror effect in a broadband sense rather than targeting a specific bandgap as in similar periodic metamaterial counterparts.

Figure 1(a) displays the schematic of the EAM-based piezoelectric energy harvesting concept. A point source is located at one focus of the semi-ellipse while the energy harvester is located at the other focus (which is the point of wave focusing in space). The frequency range of analysis is 25–150 kHz, a range where only the S_0 and the A_0 Lamb wave modes propagate in the plate. The EAM design, and specifically the spacing of the stubs along the ellipse (here chosen as 10 mm), is based on the characteristics of the A_0 mode, given its predominantly out-of-plane polarization, which makes its measurement particularly convenient.

The performance of the EAM is first investigated numerically through simulations that predict the wavefield generated by a point source located at one focal point of the ellipse and estimate the focusing effect of the scatterers. A multiple-scattering problem is formulated whereby the plate is an infinite medium, and each stub acts as a point scatterer. In the considered formulation, the plate response at location

^{a)}Author to whom correspondence should be addressed. Electronic mail: alper.erturk@me.gatech.edu.

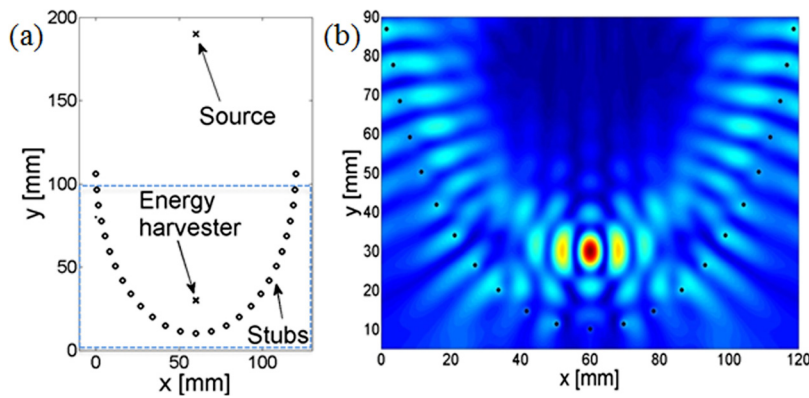


FIG. 1. (a) Schematic of the EAM configuration depicting the location of the point source of excitation and of the piezoelectric energy harvester; (b) detail of the simulated RMS displacement distribution over the region bounded by the dashed rectangle in (a) exhibiting focusing of the wave energy at the location of the energy harvester.

w due to a point source at \mathbf{x}_s is evaluated through a Green's function formalism,²⁹ which gives

$$w(\mathbf{x}, \omega) = g_0(\omega) \mathcal{G}(\mathbf{x}, \mathbf{x}_s, \omega), \quad (1)$$

where $w(\mathbf{x}, \omega)$ denotes the plate's out-of-plane displacement while $g_0(\omega)$ is the amplitude of the excitation at frequency ω . Here, the Green's function \mathcal{G} is approximated as³⁰

$$\mathcal{G}(\mathbf{x}, \mathbf{x}_s, \omega) = j\pi^2 H_0^{(1)}(kr_S), \quad (2)$$

where $H_0^{(1)}$ is the Hankel function of the first kind and order 0, and $r_S = |\mathbf{x} - \mathbf{x}_s|$ is the distance of the considered point from the source. Furthermore, k is the wavenumber of the considered wave mode (A_0 in this case), which is related to frequency through the corresponding dispersion branch $k = k(\omega)$ of the plate's Lamb wave spectrum. The scatterers are modeled as additional sources that provide an excitation proportional to the amplitude of the wavefield at their location. The resulting wavefield at location \mathbf{x} can, therefore, be expressed as²⁹

$$w(\mathbf{x}, \omega) = w^*(\mathbf{x}, \omega) + \sum_{m=1}^M w^*(\mathbf{x}_m, \omega) \tau_m \mathcal{G}(\mathbf{x}, \mathbf{x}_m, \omega), \quad (3)$$

where τ_m is the scattering coefficient for the m th scatterer at \mathbf{x}_m while $w^*(\mathbf{x}, \omega)$ denotes the wavefield at \mathbf{x} , which is the result of contributions from the applied excitation and of other scattering events accounted for through the repeated application of Eqs. (1) and (2).

The simulations consider the configuration of Fig. 1(a), where an aluminum plate of 1 mm thickness is excited at the upper focus of the ellipse by a 4-cycle tone burst of central frequency of 50 kHz. For simplicity, the scattering coefficient is set to unity, and a single mutual interaction between scatterers is allowed. This choice is based on a limited parametric study, which investigated the predicted wavefield for different numbers of mutual interactions, and showed that for the considered configuration, a single interaction provides a good compromise between computational efficiency and predictive capability of the model. Figure 1(b) displays the spatial distribution of the root mean square (RMS) of a portion of the wavefield (note that the initial source field has been removed for clarity) and illustrates the focusing of the wave energy at the location of the energy harvester.

Next, the performance of the EAM-based wave energy harvester is investigated experimentally and compared to

that of a *free* wave energy harvester (see Figs. 2(a) and 2(b)) to evaluate the enhancement in energy harvesting performance provided by the EAM. In the experiments, the source and the energy harvester are both piezoelectric disks of 5 mm diameter and 0.4 mm thickness (STEMiNC Corp.) bonded to a 1 mm thick aluminum plate. The plate is excited by sinusoidal burst (4 cycles) at selected frequencies, provided to the piezoelectric source by a function generator (Agilent 33220A) through a voltage amplifier (Trek Model PZD350). The resulting wavefield is measured by a Polytec PSV-400 scanning laser vibrometer. Wavefield images and RMS distributions are obtained by recording the plate response over a grid of points, which covers the region containing the EAM. Proper phasing of excitation and triggering of the laser measurements allows the reconstruction of the wavefield and the evaluation of the RMS through integration in time of the recorded response. Figure 3 displays experimental RMS distribution of the velocity field for excitation at 50 kHz, shows a very good agreement with the simulations (Fig. 1(b)), and clearly demonstrates the focusing effect of the EAM.

The broadband focusing characteristics of the EAM are investigated by performing experiments at various frequencies in the 25–150 kHz range. At each frequency, the response of the plate is measured along the center line of the EAM (the vertical line $x = 60$ mm in Fig. 3), which coincides with the major axis of the elliptical layout. The results are summarized in Fig. 4, which shows the variation of the normalized wave amplitude along the centerline and as a function of excitation frequency. Amplitude normalization is conducted in terms of the amplitude at the location of the

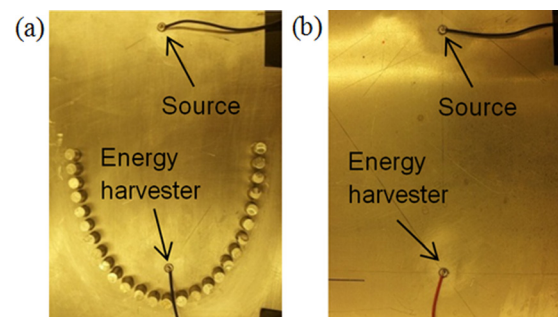


FIG. 2. Experimental configurations: (a) Energy harvester located at the focus of the EAM configuration and (b) free energy harvester configuration in the absence of the EAM for comparison of the generated electrical power for the same wave excitation and the same distance from the source.

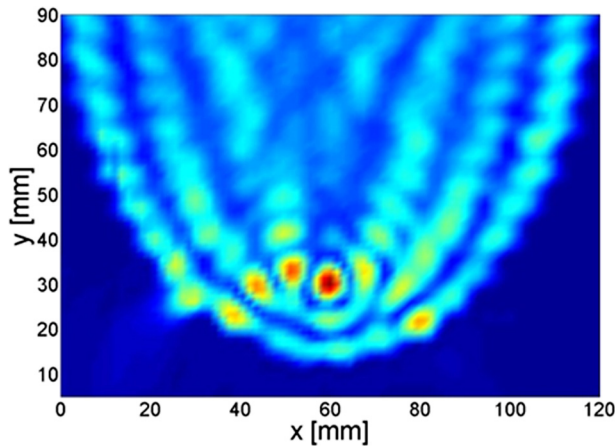


FIG. 3. Experimentally measured RMS velocity field for excitation at 50 kHz (the source region is excluded) for the EAM configuration shows wave focusing at the location of the energy harvester.

source, in order to eliminate the influence of frequency dependent coupling between the piezo disk and the plate.³¹ The results clearly illustrate how the piezoelectric source (located at $y = 190$ mm) creates a velocity field that is amplified by the acoustic mirror to create a second peak at the focal point of the ellipse (located at $y = 30$ mm). The amplitude of this second peak varies with frequency and reaches its maximum values around 50 kHz. Above this frequency, a general decaying trend for the amplitude at the focus is observed, which may be explained by decreasing wavelength of the A_0 mode with frequency. This leads to a reduced effectiveness of the EAM, which is due to the effect of the spacing of the stubs (in this case 10 mm along the elliptical path), which becomes of the order of the A_0 wavelength at frequencies higher than 50 kHz. For reference purposes, at 50 kHz, the A_0 mode propagates in a 1 mm thick aluminum plate at a velocity of 1.33 mm/ μ s, with a wavelength of 13.8 mm.

Electrical power generation (resistor sweep) experiments are conducted for the configurations (Fig. 2) with and without the EAM. The voltage signal from the energy harvesting piezoelectric disk is placed across a resistive decade box (IET Labs Inc.) in parallel with a Tektronix TDS2024 oscilloscope. A graphical user interface collects the oscilloscope time signal with an Agilent 82357 A, and the average power is calculated with knowledge of the swept resistance values. Figure 5(a) shows the time history of the voltage output across an electrical load of 4.5 k Ω at 50 kHz (which is

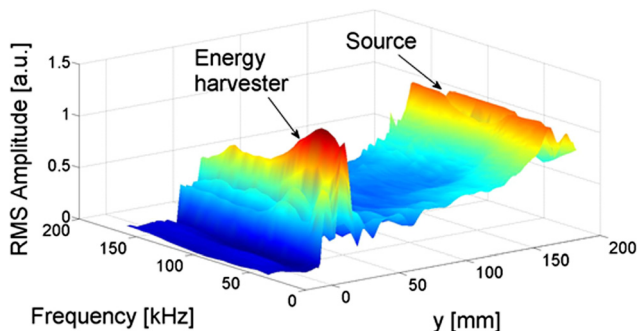


FIG. 4. Normalized experimental RMS velocity field along the major axis ($x = 60$ mm) of the semi-ellipse for the frequency range of 25–150 kHz showing the locations of the source and the energy harvester.

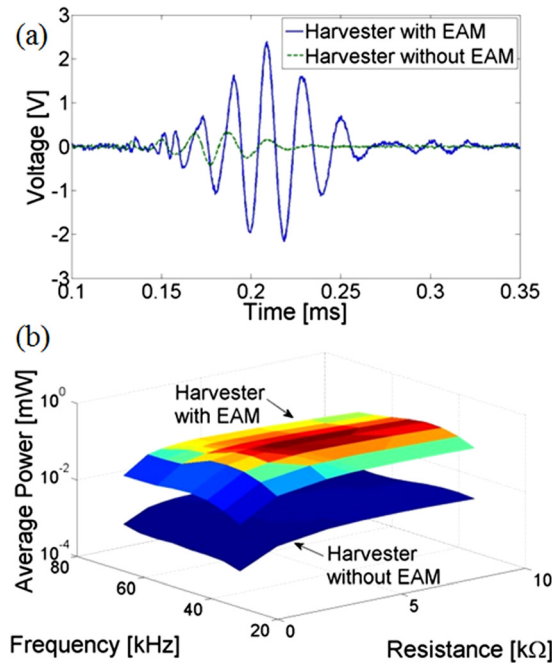


FIG. 5. Performance comparison of the energy harvesters with and without the EAM configuration: (a) voltage output histories at 50 kHz for 4.5 k Ω ; (b) power versus load resistance and frequency surfaces for the frequency range of 30–70 kHz covering the region of the optimal electrical load at each frequency.

around the optimal electrical load estimated based on the relation $R = 1/\omega C$ where the excitation frequency and the piezoelectric capacitance are $\omega = 10^5 \pi$ rad/s and $C = 0.76$ nF). The advantage of the EAM can be seen in Fig. 5(a), where the voltage signal is greatly increased as compared to the free energy harvester without the EAM. Note that the amplified signal is also slightly delayed as the vibrations travel a longer distance from one focus to the elliptical surface to the other focus as compared to traveling directly between the two foci.

Further energy harvesting experiments are conducted for the frequency range of 30–70 kHz. Figure 5(b) exhibits that the EAM-based configuration dramatically increases the power harvested over a broad range of excitation frequencies. The maximum power generated by the EAM-based energy harvester occurs at 50 kHz and 4.5 k Ω with 126 μ W, whereas the free harvester showed a maximum at 45 kHz and 4.5 k Ω producing 3.3 μ W of power. Across all resistance levels, the greatest increase is at 50 kHz with over 1.5 orders of magnitude greater power over the free harvester case. Finally, across all resistance and frequency levels, the system showed an average of 3075% increase over the free harvester case, demonstrating that even though it is best suited for use at 50 kHz, this system exhibits broadband characteristics over the frequency range analyzed in agreement with Fig. 4.

Dramatic enhancement of structure-borne energy harvesting has been reported by combining piezoelectric energy harvesting with the acoustic mirror effect created by an EAM configuration. The proposed configuration increases the harvested power more than an order of magnitude over a broad range of excitation frequencies. Alternative acoustic mirror configurations (such as a parabolic mirror) are of interest for future research in order to focus and harvest

structure-borne plane waves rather than point sources. Analogous mirroring concepts can also be employed for harvesting air-borne waves¹⁶ using polymer-based piezoelectric materials.

- ¹N. S. Hudak and G. G. Amatuucci, *J. Appl. Phys.* **103**, 101301 (2008).
- ²K. A. Cook-Chennault, N. Thambi, and A. M. Sastry, *Smart Mater. Struct.* **17**, 043001 (2008).
- ³A. Erturk, J. Hoffmann, and D. J. Inman, *Appl. Phys. Lett.* **94**, 254102 (2009).
- ⁴G. Litak, M. I. Friswell, and S. Adhikari, *Appl. Phys. Lett.* **96**, 214103 (2009).
- ⁵S. C. Stanton, C. C. McGehee, and B. P. Mann, *Appl. Phys. Lett.* **95**, 174103 (2009).
- ⁶A. Erturk and D. J. Inman, *Piezoelectric Energy Harvesting* (Wiley, Chichester, UK, 2011).
- ⁷S. Roundy, P. Wright, and J. Rabaey, *Energy Scavenging for Wireless Sensor Networks* (Kluwer, Boston, 2004).
- ⁸P. Mitcheson, P. Miao, B. Start, E. Yeatman, A. Holmes, and T. Green, *Sens. Actuators, A* **115**, 523–529 (2004).
- ⁹P. Glynn-Jones, M. J. Tudor, S. P. Beeby, and N. M. White, *Sens. Actuators, A* **110**, 344–349 (2004).
- ¹⁰D. Arnold, *IEEE Trans. Magn.* **43**, 3940–3951 (2007).
- ¹¹L. Wang and F. G. Yuan, *Smart Mater. Struct.* **17**, 045009 (2008).
- ¹²X. Xing, J. Lou, G. M. Yang, O. Obi, C. Driscoll, and N. X. Sun, *Appl. Phys. Lett.* **95**, 134103 (2009).
- ¹³S. Koh, X. Zhao, and Z. Suo, *Appl. Phys. Lett.* **94**, 262902 (2009).
- ¹⁴M. Aureli, C. Prince, M. Porfiri, and S. D. Peterson, *Smart Mater. and Struct.* **19**, 015003 (2010).
- ¹⁵S. B. Horowitz, M. Sheplak, L. N. Cattafesta, and T. Nishida, *J. Micro-mech. Microeng.* **16**, S174 (2006).
- ¹⁶L. Y. Wu, L. W. Chen, and C. M. Liu, *Appl. Phys. Lett.* **95**, 013506 (2009).
- ¹⁷C. J. Rupp, M. L. Dunn, and K. Maute, *Appl. Phys. Lett.* **96**, 111902 (2010).
- ¹⁸A. Erturk, W. G. R. Vieira, C. De Marqui, Jr., and D. J. Inman, *Appl. Phys. Lett.* **96**, 184103 (2010).
- ¹⁹D. St. Clair, A. Bibo, V. R. Sennakesavababu, M. F. Daqaq, and G. Li, *Appl. Phys. Lett.* **96**, 144103 (2010).
- ²⁰S. D. Kwon, *Appl. Phys. Lett.* **77**, 164102 (2010).
- ²¹A. Giacomello and M. Porfiri, *J. Appl. Phys.* **109**, 084903 (2011).
- ²²S. Guenneau, A. Movchan, G. Petursson, and S. A. Ramakrishna, *New J. Phys.* **9**, 339 (2007).
- ²³T. C. Wu, T. T. Wu, and J. C. Hsu, *Phys. Rev. B* **79**, 104306 (2009).
- ²⁴M. Ruzzene and F. Scarpa, *Phys. Status Solidi B* **242**, 665–680 (2005).
- ²⁵M. Ruzzene, F. Scarpa, and F. Soranna, *Smart Mater. Struct.* **12**, 363–372 (2003).
- ²⁶A. Sukhovich, L. Jing, and J. H. Page, *Phys. Rev. B* **77**, 014301 (2008).
- ²⁷D. Torrent and J. Sánchez-Dehesa, *New J. Phys.* **9**, 323 (2007).
- ²⁸M. Oudich, M. Senesi, M. B. Assouar, M. Ruzzene, J. H. Sun, B. Vincent, Z. Hou, T. T. Wu, *Phys. Rev. B* **84**, 165136 (2011).
- ²⁹E. Baravelli, M. Senesi, M. Ruzzene, L. De Marchi, and N. Speciale, *IEEE Trans. Ultrason. Ferroelectr. Freq. Control* **58**, 1430–1441 (2011).
- ³⁰K. F. Graff, *Wave Motion in Elastic Solids* (Dover, New York, 1975).
- ³¹M. Collet, M. Ruzzene, and K. Cunefare, *Smart Mater. Struct.* **20**, 025020 (2011).